Prediction of laser cutting parameters for polymethylmethacrylate sheets using random vector functional link network integrated with equilibrium optimizer

Article *in* Journal of Intelligent Manufacturing · June 2021

DOI: 10.1007/s10845-020-01617-7

CITATIONS
9

READS
269

5 authors, including:

Ammar Elsheikh
Tanta University
82 PUBLICATIONS **1,399** CITATIONS
SEE PROFILE

Taher Atia
Kafrelsheikh University
11 PUBLICATIONS **74** CITATIONS
SEE PROFILE

Ezzat A. Showaib
Tanta University
29 PUBLICATIONS **148** CITATIONS
SEE PROFILE

Mohamed Elsayed Abd Elaziz
Zagazig University
209 PUBLICATIONS **3,595** CITATIONS
SEE PROFILE

Journal of Intelligent Manufacturing
https://doi.org/10.1007/s10845-020-01617-7

Prediction of laser cutting parameters for polymethylmethacrylate sheets using random vector functional link network integrated with equilibrium optimizer

Ammar H. Elsheikh[1] · Taher A. Shehabeldeen[2,3] · Jianxin Zhou[2] · Ezzat Showaib[1] · Mohamed Abd Elaziz[4]

Received: 22 January 2020 / Accepted: 26 June 2020

Abstract

In this paper, an enhanced random vector functional link network (RVFL) algorithm was employed to predict kerf quality indices during CO_2 laser cutting of polymethylmethacrylate (PMMA) sheets. In the proposed model, the equilibrium optimizer (EO) is used to augment the prediction capability of RVFL via selecting the optimal values of RVFL parameters. The predicting model includes four input variables: gas pressure, sheet thickness, laser power, and cutting speed, and five kerf quality indices: rough zone ratio, widths of up and down heat affected zones, maximum surface roughness, and kerf taper angle. The experiments were designed using Taguchi L18 orthogonal array. The kerf surface contains three main zones: rough, transient, and smooth zones. The results of conventional RVFL as well as modified RVFL-EO algorithms were compared with experimental ones. Seven statistical criteria were used to assess the performance of the proposed algorithms. The results indicate that the RVFL-EO model has the predicting ability to estimate the laser-cutting characteristics of PMMA sheet.

Keywords Laser cutting · Kerf quality indices · Random vector functional link network · Equilibrium optimizer

Introduction

In recent years, polymeric materials such as polymethylmethacrylate (PMMA) have been used as promising alternatives to conventional metallic materials. That is due to their featured properties such as cheapness, high strength to weight ratio, low thermal conductivity, resilience, toughness, resistance to corrosion, low electrical conductivity, and easy processing (Bao et al. 2010; Leal-Junior et al. 2018a, b; Leal-Junior et al. 2019; Showaib and Elsheikh 2020). PMMA is one of the most common used thermoplastic polymeric materials in different engineering applications such as car windows, light-emitting diode casings, optical lenses, LCD backlit display panels, smartphone screens, optical fibers, lighting fixtures and electronics (Kim 2005; Huang et al. 2002).

Conventional machining process of different engineering materials has been constrained due to several critical issues such as complex shape of work material, strict design prerequisite, and the rapid development of advanced engineering materials (Dubey and Yadava 2008; Elsheikh et al. 2018; Salman et al. 2019). Advanced machining process such as ion beam machining, laser beam machining (LBM), plasma beam machining, electron beam machining, and water jet machining are progressively being used as alternatives to conventional machining techniques (Davim 2013; Gonzalez-Val et al. 2020; Jagadish and Ray 2019; Ergur and Oysal 2015). Laser beam machining is widely used in fine sheet cutting of different materials such as metals, glass, and plastics because of its high intensity and precision. The laser beam is directed to the workpiece surface in which it is absorbed and its energy is converted into heat. A relative

✉ Ammar H. Elsheikh
ammar_elsheikh@f-eng.tanta.edu.eg

✉ Jianxin Zhou
zhoujianxin@hust.edu.cn

[1] Department of Production Engineering and Mechanical Design, Faculty of Engineering, Tanta University, Tanta 31527, Egypt

[2] State Key Laboratory of Materials Processing and Die & Mould Technology, Huazhong University of Science and Technology, Wuhan 430047, China

[3] Department of Mechanical Engineering, Faculty of Engineering, Kafrelsheikh University, Kafrelsheikh 33516, Egypt

[4] Department of Mathematics, Faculty of Science, Zagazig University, Zagazig 44519, Egypt

Published online: 06 July 2020

motion between the laser beam and the workpiece is controlled to cut the material in the required shape with good surface finish compared to other conventional machining techniques.

Thermoplastics and plastics of different thicknesses can be cut using laser beams by simply adjusting the intensity of the beam, the relative speed between workpiece and the laser source, the standoff distance between the laser source and the workpiece surface, and the pressure of assist gas (Elsheikh et al. 2019). Machining of plastic materials by laser beam has been increasingly used in several industries due to high cut edge quality and high process reliability. Cutting quality depends on the process parameters such as sheet thickness, cutting speed, standoff distance, pressure of assist gas, laser power and mode of operation (pulsed mode or continuous wave). Among different types of lasers, Nd: YAG and CO_2 lasers have good efficiency, good beam quality, and low beam power. The application of CO_2 laser cutting has been introduced by Bai (2004), they have reported that CO_2 laser with low power (60 W) can be utilized for cutting non-metallic materials such as wood, rubber, particle board, and plastics. For all investigated materials, the input power of the laser has a nonlinear relationship with the thickness of the cut sheet. Choudhury and Shirley (2010) have examined CO_2 laser cutting of three polymeric materials PMMA, polycarbonate (PC) and polypropylene (PP). They concluded that the cutting quality in case of PMMA is much better than that of PC and PP. In the case of PMMA and PP, the pressure of assist air had an insignificant effect on the heat affected zone compared to PC. Davim et al. (2008) investigated cutting quality (dimensional accuracy, surface roughness and HAZ) of PMMA with CO_2 laser for both linear and complex two-dimensional pattern of the work material. They concluded that HAZ was relatively low (0.12–0.37 mm) without any burr formation.

Wang et al. (2008) investigated the effects of the pressure of oxygen assist gas and repetition rate on HAZ during laser cutting of FR4 and BT/epoxy based PCB substrates. Caiazzo et al. (2005) investigated three thermoplastic polymers (polyethylene (PE), PP and PC) with thickness range between 2 and 10 mm. They studied cutting speed, laser power, thickness of work materials, and gas pressure as the input parameters. They concluded that laser cutting workability of PE, PP, and PC was low, medium, and high, respectively. Prakash and Kumar (2017) established an analytical model of multi-pass CO_2 laser processing of PMMA sheet. The results were validated experimentally. The change in the thermo-physical properties of the material due to the cutting process was monitored. Effects of number of passes on the microchannel geometry, surface roughness, and HAZ were investigated for different laser power intensity. Multi-pass processing showed many advantages over single-pass processing such as better surface roughness of microchannel walls, high aspect ratios, smaller HAZ, and reasonable kerf taper.

Narrow kerf width with minimum burn out of medium density fiber board was achieved using pulsed CO_2 laser (Lum et al. 2000). Mathew et al. (1999) optimized the laser cutting process of carbon fiber reinforced plastics composites considering the kerf geometry and HAZ using response surface methodology. The CO_2 laser cutting of engineering plastics was investigated by Kurt et al. (2009). The optimal cutting speed, laser power, and gas pressure that minimize the surface roughness and maximize the dimensional accuracy of the kerf have been obtained. It was reported that while the cutting speed and the laser power have a significant effect on the surface roughness and the dimensional accuracy, the gas pressure has a negligible effect on them. Moreover, a nonlinear relationship between surface roughness of the cut surface and cutting speed was recorded.

Davim et al. (2008) investigated the effects of cutting speed and laser power on the quality of the generated kerf during laser cutting of three polymeric materials: PMMA, PC, and PP. Three kerf characteristics were considered: surface roughness, presence of burr, and HAZ. It was reported that HAZ decreases with laser power and increases with cutting speed. The laser cutting of metals have been also widely investigated. Rao and Yadava (2009) investigated pulsed Nd:YAG laser cutting of Inconel 718 sheet considering four different process parameters: pulse frequency, pulse width, oxygen pressure, and cutting speed. Three kerf characteristics have been considered: kerf width, deviation, and taper. Dubey and Yadava (2008) investigated pulsed Nd:YAG laser cutting of SUPERNI 718 using a hybrid Taguchi method considering the quality of the kerf geometry. Sharma et al. (2010; Sharma and Yadava 2011) experimentally investigated the kerf quality indices during Nd:YAG laser cutting of nickel-based superalloy sheet using Taguchi orthogonal array. Chien and Hou (2007) applied Taguchi method to explore the formed recasting layers during Nd:YAG laser drilling of Inconel 718. Prakash and Kumar (2018) investigated CO_2 laser based raster scanning process for PMMA. They developed a theoretical model for predicting micromachined profile and depth based on conservation of energy principal. The

developed model was derived based on superposition of Gaussian beams and principal of energy conservation. A good agreement was observed between the predicted depth and evolved micro-structure profile and the actual depths and profile with maximum prediction error less than 7.23%. Alizadeh and Omrani (2019) have successfully constructed a robust optimization approach to handle uncertainty in neural network results. First, they used Taguchi method to design the experiments, then some experiments are applied, and other experiments were assessed by a back-propagation neural network (BPNN) technique. Finally, the best parameters are selected by using optimal robust data envelopment analysis (RDEA) model. Volpe et al. (2019) established a prediction model to describe the relationship between the response variable depth and the main laser parameters for femtosecond-laser micro milling process of PMMA in terms of depth of removed material. They concluded that the laser pulse energy is the main parameter that affects the milling depth. D'Addona et al. (2016) constructed an artificial neural network (ANN) model to predict the surface roughness and the depth in CO_2 laser milling of PMMA. A good agreement between the model and the experimental data was achieved.

Shrivastava and Pandey (2018) developed a multi-objective regression model which integrated with a genetic algorithm to optimize the kerf width, kerf deviation, and kerf taper in the laser cutting of Inconel-718 sheet. They concluded that an improvement of 10.63%, 88% and 42.15% in kerf width, kerf deviation, and kerf taper, respectively was observed. Gautam and Pandey (2018) applied a teaching learning algorithm to acquire the minimum kerf deviation at bottom and top sides of the Nd:YAG laser cutting system on Kevlar-29 composite laminates, different laser cutting parameters such as pulse frequency, lamp current, compressed air pressure, pulse width, and cutting speed on top kerf and bottom kerf deviation have been studied, they concluded that the machining performance of laser beam cutting process has been remarkably improved.

In this work, a new technique was employed to improve the prediction of different laser cutting quality indices (surface roughness, area of rough zone, HAZ, and kerf taperness). The proposed technique consists of a random vector functional link network (RVFL) integrated with Equilibrium Optimizer (EO) (Faramarzi et al. 2019). The former algorithm is used to predict the laser cutting quality indices based on different cutting parameters, while the latter is used to augment the performance of the predictive model. The proposed algorithm was trained using experimental results planned using Taguchi method. The performance of the proposed RVFL-EO algorithm was compared with that of conventional RVFL using different statistical criteria.

Mathematical modeling

Random vector functional link network

RVFL has been proposed as a good alternative to conventional artificial neural networks that suffers from overfitting problems (Huang et al. 2020; Elsheikh et al. 2020; Elsheikh et al. 2013). In this section, a general overview of the RVFL is introduced (Zhang and Yang 2020). RVFL is a type of single layer feedforward neural network but there exists a link between the input neuron and the neuron at the output layer (see Fig. 1). The steps of RVFL can be formulated as follows: the first step is to receive the input data that contains the features (x_i) and labels (y_i). Then these data are applied to the nodes at the input layer and passed through the hidden layer which called enhancement nodes that produce an output computed as

$$O_j\left(\alpha_j x_i + \beta_j\right) = \frac{1}{1 + e^{-\left(\alpha_j x_i + \beta_j\right)}}, \beta_j \in [0, S], \alpha_j \in [-S, S] \quad (1)$$

In Eq. (1), β_j represents the bias and α_j refers to the weight between the input layer and enhancement nodes, while, S is a scale factor. Thereafter, the RVFL generate the final output which is the estimation of y_i and this depends on the weight w as defined in Eq. (2)

$$Z = F = \left[F_1, F_2\right] w, \quad w \in R^{n+P}, \quad (2)$$

where,

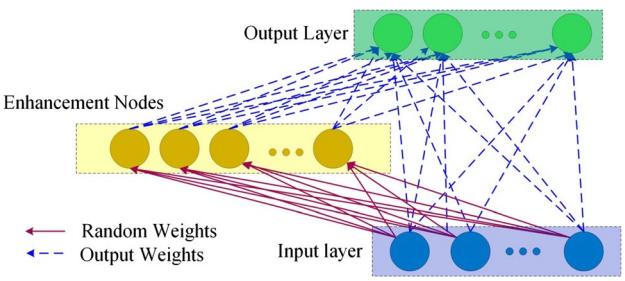

Fig. 1 The structure of RVFL network

$$F_1 = \begin{bmatrix} x_{11} & \cdots & x_{1n} \\ \vdots & \ddots & \vdots \\ x_{N1} & \cdots & x_{Nn} \end{bmatrix}, \quad F_2 = \begin{bmatrix} G_1(\alpha_1 x_1 + \beta_1) & \cdots & G_P(\alpha_P x_1 + \beta_P) \\ \vdots & \ddots & \vdots \\ G_1(\alpha_1 x_N + \beta_1) & \cdots & G_P(\alpha_P x_N + \beta_P) \end{bmatrix} \tag{3}$$

The next process is to update w using the following equation

$$w = F^{\dagger} Z \tag{4}$$

where †, represents the Moore–Penrose pseudo-inverse.

Equilibrium optimizer

The equilibrium optimizer (EO) is a metaheuristic (MH) optimization algorithm belongs to mathematical type which mixes dynamic mass balance on a control volume (Faramarzi et al. 2019). The EO begins by put the initial value for N particles (C) using the following equation

$$C_i = LB + rand \times (UB - LB), \tag{5}$$

where C_i represents the concentration of the particles $i-$. LB and UB are the bombardiers of the search space. The $rand \in [0, 1]$ is uniform random value.

The particles C are assessed by computing the fitness function followed by determining the equilibrium solutions after sorting them. Following (Faramarzi et al. 2019), the equilibrium solutions are formulated as in the following equation.

$$C_{eq} = \left\{ C_{eq}^1, C_{eq}^2, C_{eq}^3, C_{eq}^4, C_{eq}^{avg} \right\} \tag{6}$$

where $C_{eq}^1, C_{eq}^2, C_{eq}^3$, and C_{eq}^4 are the four best solutions and C_{eq}^{avg} is their average. The solutions during the updating process select a random one from $C_{eq,p}$ to update their concentrations.

The next step is to update the exponential term (F) using the following equation

$$F = a_1 sign(r - 0.5)\left(e^{-\lambda t} - 1\right), \quad t = \left(1 - \frac{iter}{\max\_iter}\right)^{\frac{a_2 \times iter}{\max\_iter}} \tag{7}$$

where λ is the turnover rate, while, the a_1 and a_2 are constants used to control the exploration and exploitation, respectively. $r \in [0, 1]$ random value and $sign(r - 0.5)$ are used to manage the direction of exploration and exploitation.

The next step is to update the Generation rate (G) as formulated in the following equation.

$$G = G_0 F, \quad G_0 = G_{CP}\left(C_{eq} - \lambda C\right) \tag{8}$$

where G_{CP} represents the parameter that controls the generation rate and it is defined as:

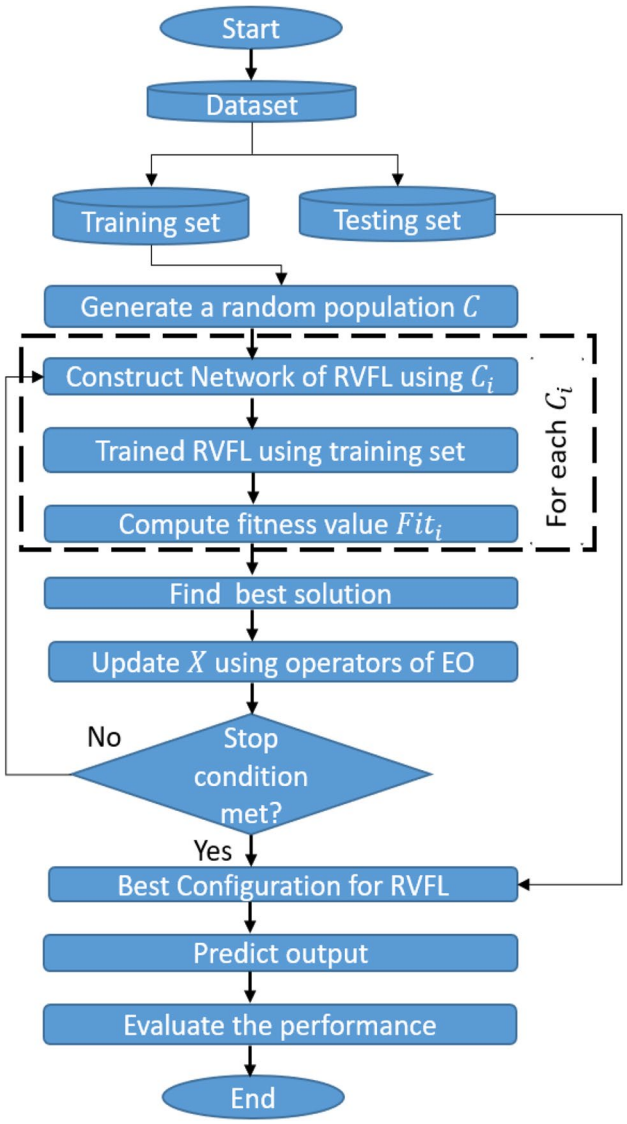

Fig. 2 The RVFL-EO for prediction the laser cutting quality indices

$$G_{CP} = \begin{cases} 0.5 r_1 & r_2 \geq GP \\ 0 & otherwise \end{cases} \tag{9}$$

GP is the generation probability. According to the G and F the solution i can be updated using the following equation

$$C_i = C_{eq} + \left(C_i - C_{eq}\right) \times F + (1 - F)\frac{G}{\lambda V} \tag{10}$$

where V represents considered unit. The full steps of the EO are given in Algorithm 1.

Algorithm 1: EO algorithm

Input the number of solutions N and the total number of iterations Max_iter

Set the value for the parameters $a_1 = 2, a_2 = 1, and\ GP = 0.5$

Set the initial value for N particles

Set initial value for the equilibrium candidates C_{eq}

Set Iter=1;

While Iter< Max_iter

For i=1: N

Compute fitness value for C_i

If $fit(C_i) < fit(C_{eq}^1)$

$C_{eq}^1 = C_i$ and $fit(C_{eq}^1) = fit(C_i)$

Else-if $fit(C_i) < fit(C_{eq}^2)$& $fit(C_i) > fit(C_{eq}^1)$

$C_{eq}^2 = C_i$ and $fit(C_{eq}^2) = fit(C_i)$

Else-if $fit(C_i) < fit(C_{eq}^3)$& $fit(C_i) > fit(C_{eq}^1)$&$fit(C_i) > fit(C_{eq}^2)$

$C_{eq}^3 = C_i$ and $fit(C_{eq}^3) = fit(C_i)$

Else-if $fit(C_i) < fit(C_{eq}^4)$& $fit(C_i) > fit(C_{eq}^1)$ &$fit(C_i) > fit(C_{eq}^2)$&$fit(C_i) > fit(C_{eq}^3)$

$C_{eq}^4 = C_i$ and $fit(C_{eq}^4) = fit(C_i)$

End if

End (For)

Update the $C_{eq}^{avg} = (C_{eq}^1 + C_{eq}^2 + C_{eq}^3 + C_{eq}^4)/4$

Update C_{eq} as defined in Eq. (6)

Update F and G

Update C_i using Eq. (10) and with Randomly select one solution from C_{eq}.

End While

Return the best solution.

The proposed RVFL-EO method

The integration between the conventional ANN algorithms and the advanced metaheuristic optimization techniques to enhance the prediction capabilities of the ANN has been reported in literature (Elaziz et al. 2019; Babikir et al. 2019; Shehabeldeen et al. 2019; Essa et al. 2020; Shehabeldeen et al. 2020; Chaki et al. 2018). Herein, the EO-RVFL method is proposed to improve the prediction of laser cutting quality indices by finding the optimal values of RVFL parameters. The EO-RVFL starts by splitting the dataset of laser cutting parameters into training and testing which represents 70% and 30%, respectively. Followed by generating a set of N solutions (C) which represent configurations for RVFL. In this study, the most significant parameters of RVFL are tested which include number of hidden neurons, activation function, and randomization method. So, the values of current solution will be generated using the following equation

$$C_{ij} = l_j + r \times \left(u_j - l_j\right), i = 1, \ldots, N, \quad j = 1, \ldots, 3, r \in [0, 1] \tag{11}$$

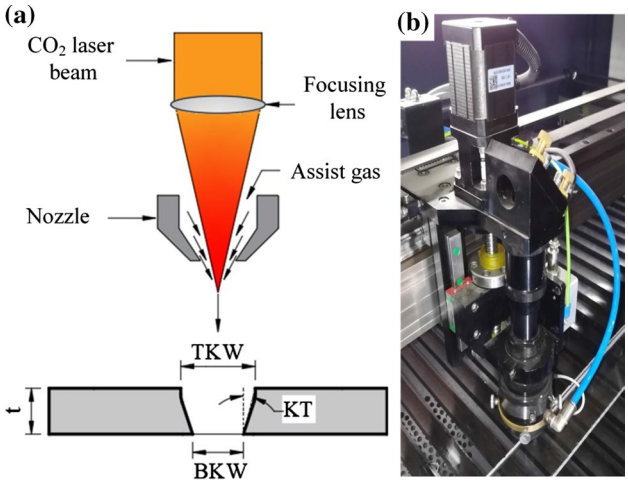

Fig. 3 **a** A schematic diagram of laser cutting process; **b** experimental setup of CO_2 laser cutting process

where u_j and l_j are the upper and lower boundaries at jth parameter, respectively. For clarity, assume the ith solution $C_i = [C_{i1}, C_{i2}, C_{i3}] = [N_h, AF, RT]$. $C_{i1} \in [1, 3000]$ is the number of hidden neurons; $C_{i2} \in \{1, 2, 3, 4, 5\}$ is the activation function (which refers to sign, tribas, sig, hardlim, and radbas, respectively). The $C_{i3} \in \{1, 2\}$ represents the randomization weights method which (Uniform or Gaussian). To illustrate this process, considering $C_i = [100, 1, 2]$ this means that the i-th configuration of RVFL consists of 100 neurons with use sign as activation function and use the Gaussian distribution to set the initial value for the weights.

The next step it to apply the training set for each configuration C_i and compute the predicted values of laser cutting quality indices (Y_P), then evaluate its performance using the following function

$$Fit_i = \sqrt{\frac{\sum_{i=1}^{Ns} \left(Y_P - Y_T\right)^2}{Ns}} \tag{12}$$

Thereafter, the best configuration C_{eq}^1 is determined and other solutions are updated according to the steps of EO algorithm (see Algorithm 1). After finishing the updating process, the testing set will be applied to best configuration to evaluate the performance of the proposed model. The full process of the EO-RVFL is given in Fig. 2.

Table 2 Cutting parameters and their levels

parameter	Gas pressure (bar)	Sheet thickness (mm)	Cutting speed (mm/min)	Laser power (W)
Level 1	1	4	100	120
Level 2	3	6	200	135
Level 3	–	12	300	150

Experimental work

Laser machine

A laser system consists of a 150 W continuous CO_2 laser and focus lens with focal length of 63 mm. A fresh hermetic and detached CO_2 laser tube was used to minimize the laser power losses due to mirror surface defects. The wavelength of the used laser is 10,600 nm. The working area of the machine is 1300 mm × 900 mm with a maximum cutting speed of 4000 mm/min. Assist gas is used with the laser beam through a nozzle diameter of 1 mm as shown in Fig. 3, it works as a shielding gas, removes molten material from the cutting zone, and protects the lens from smoke emitted due to vaporization of the material. Besides, it facilitates efficient coupling of the laser beam with the work material. The stand-off distance was set to 6 mm for all experiments.

Work material

PMMA sheets were used as a testing material with three different thickness (4, 6 and 12 mm). Thermophysical properties of PMMA are given in Table 1.

Trial runs were performed before the experimentation to identify the laser cutting parameters that affect the kerf geometry of PMMA. Four cutting parameters were used as input cutting parameters, namely; air pressure, cutting speed, thickness of PMMA sheets, and the laser beam power as they have a significant impact on the kerf geometry. Table 2 displays the input cutting parameters and their values considered for experiments. For considered parameters, the number of experiments for full factorial design is large; therefore, to reduce number of experiments, design of experiment technique is adopted. Taguchi L18 orthogonal array presented

Table 1 Thermophysical properties of PMMA

Density (kg/m3)	Heat capacity KJ Kg^{-1} K^{-1}	Thermal conductivity (W m^{-1} K^{-1})	Thermal diffusivity (m^2/s)	Coefficient of thermal expansion (K^{-1})	Melting point (K)
1188	1.42	0.193	7×10^{-7}	7×10^{-5}	433

Table 3 Design matrix (Taguchi L18 orthogonal array) used to train EO-RVFL model

Trial no.	Cutting input parameters				Measured values				
	Gas pressure (bar)	Sheet thickness (mm)	Cutting speed (m/min)	Laser power (W)	Rough zone ratio (%)	Up HAZ (mm)	Down HAZ (mm)	Max. surface roughness (μm)	Kerf taper angle (°)
1	1	4	0.1	120	93.750	0.443	0.469	14.433	1.861
2	1	4	0.2	135	66.667	0.485	0.532	10.473	1.928
3	1	4	0.3	150	54.167	0.564	0.595	7.949	1.979
4	1	6	0.1	120	32.167	0.385	0.391	12.472	0.223
5	1	6	0.2	135	21.938	0.410	0.394	9.008	0.753
6	1	6	0.3	150	18.977	0.494	0.452	9.288	1.038
7	1	12	0.1	135	45.000	0.642	0.569	22.968	0.095
8	1	12	0.2	150	22.500	0.609	0.483	25.13	0.472
9	1	12	0.3	120	18.333	0.559	0.451	12.171	0.708
10	3	4	0.1	150	100.000	0.611	0.512	25.055	1.327
11	3	4	0.2	120	100.000	0.552	0.425	15.085	1.576
12	3	4	0.3	135	100.000	0.488	0.389	18.341	1.857
13	3	6	0.1	135	100.000	0.548	0.715	19.961	0.777
14	3	6	0.2	150	91.925	0.443	0.662	14.700	0.796
15	3	6	0.3	120	55.585	0.414	0.627	11.943	0.728
16	3	12	0.1	150	79.167	0.505	0.541	17.386	0.511
17	3	12	0.2	120	45.000	0.430	0.515	23.763	0.608
18	3	12	0.3	135	28.333	0.391	0.469	16.535	0.841

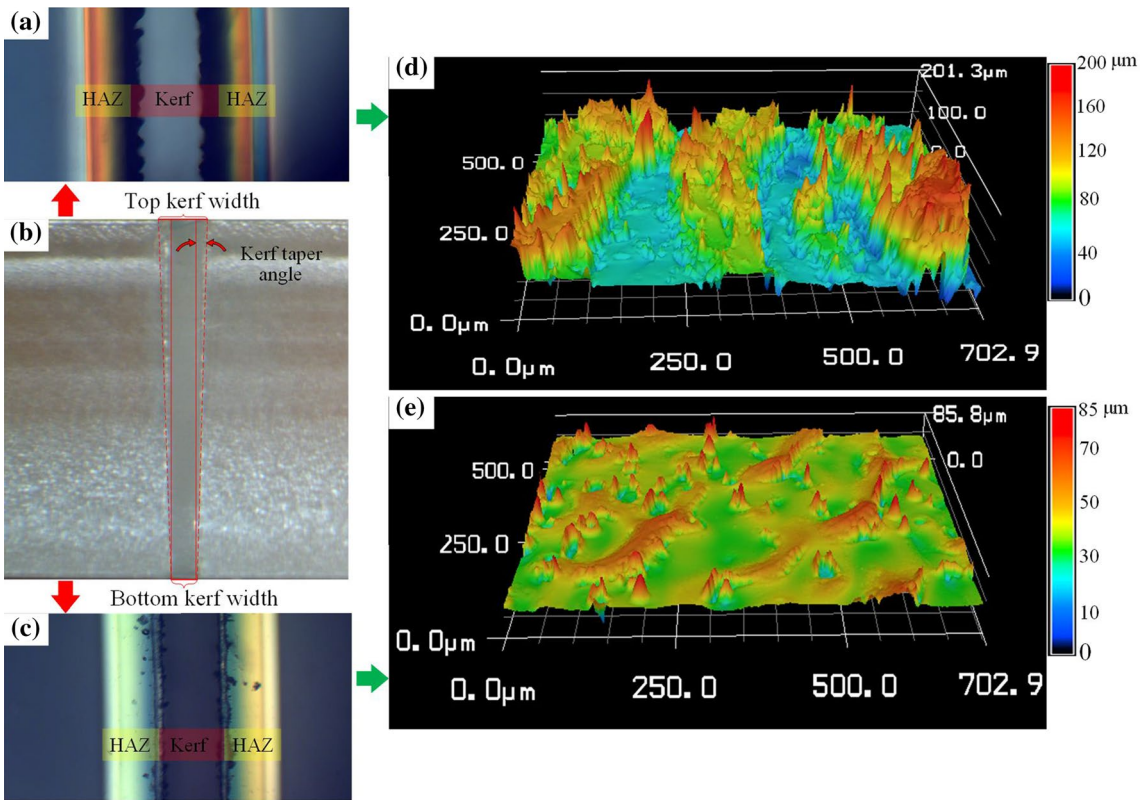

Fig. 4 Kerf quality indices of laser cutting of PMMA: **a** top view of the kerf; **b** front view of the kef; **c** bottom view of the kerf; **d** 3D view of surface texture for the top portion of the kerf; **e** 3D view of surface texture for the bottom portion of the kerf

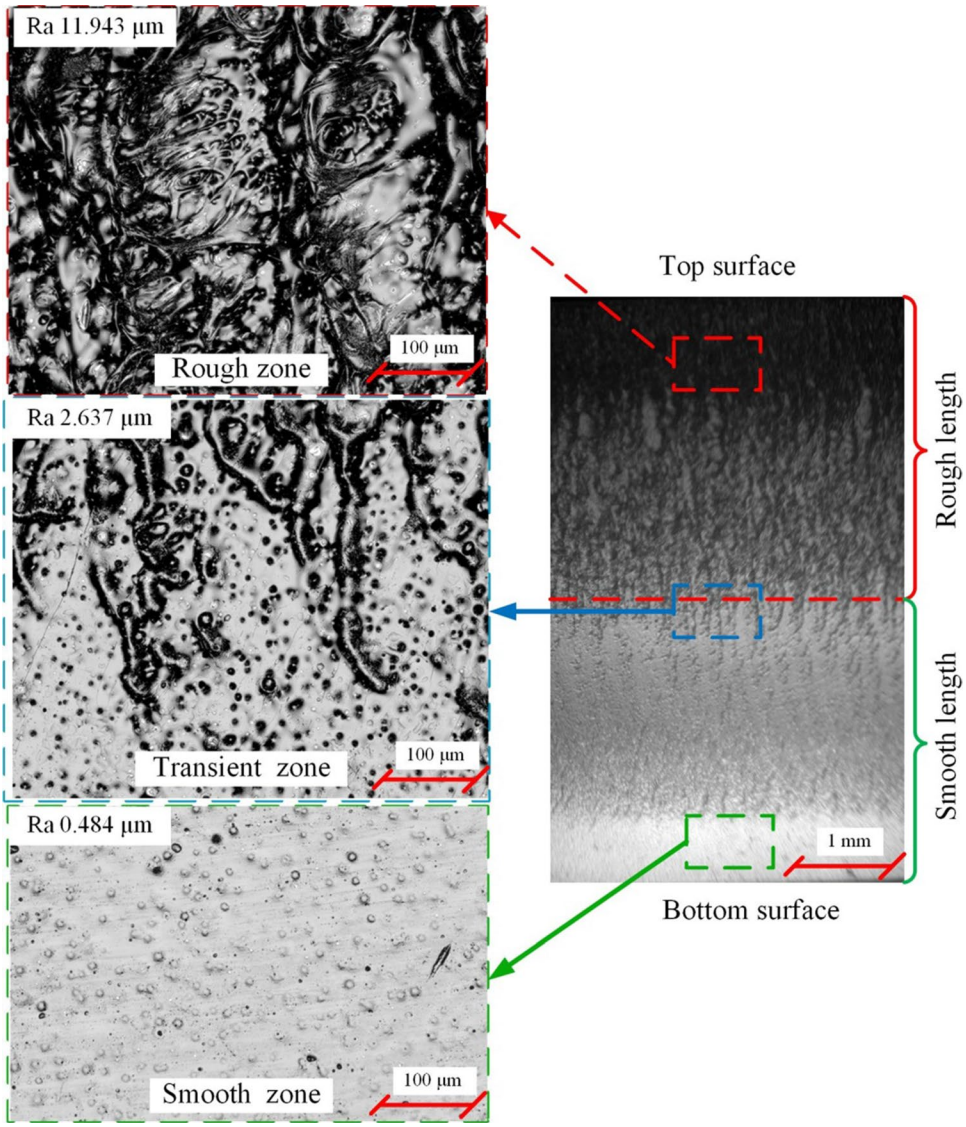

Fig. 5 Kerf surface main zones: rough, transient, and smooth zone

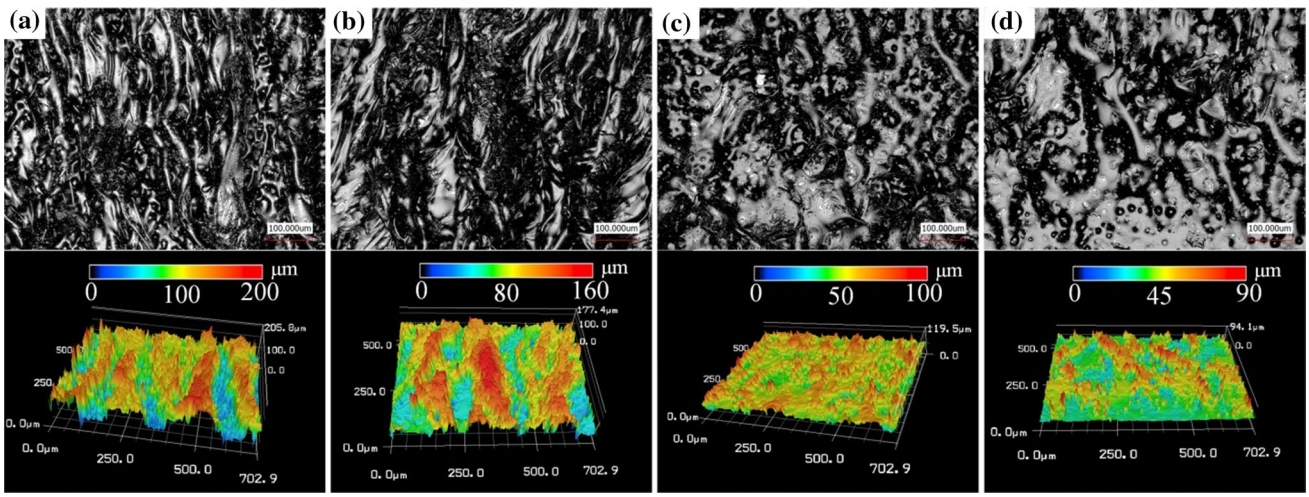

Fig. 6 Surface texture of: **a** experiment no. 10; **b** experiment no. 17; **c** experiment no. 5; **d** experiment no. 3

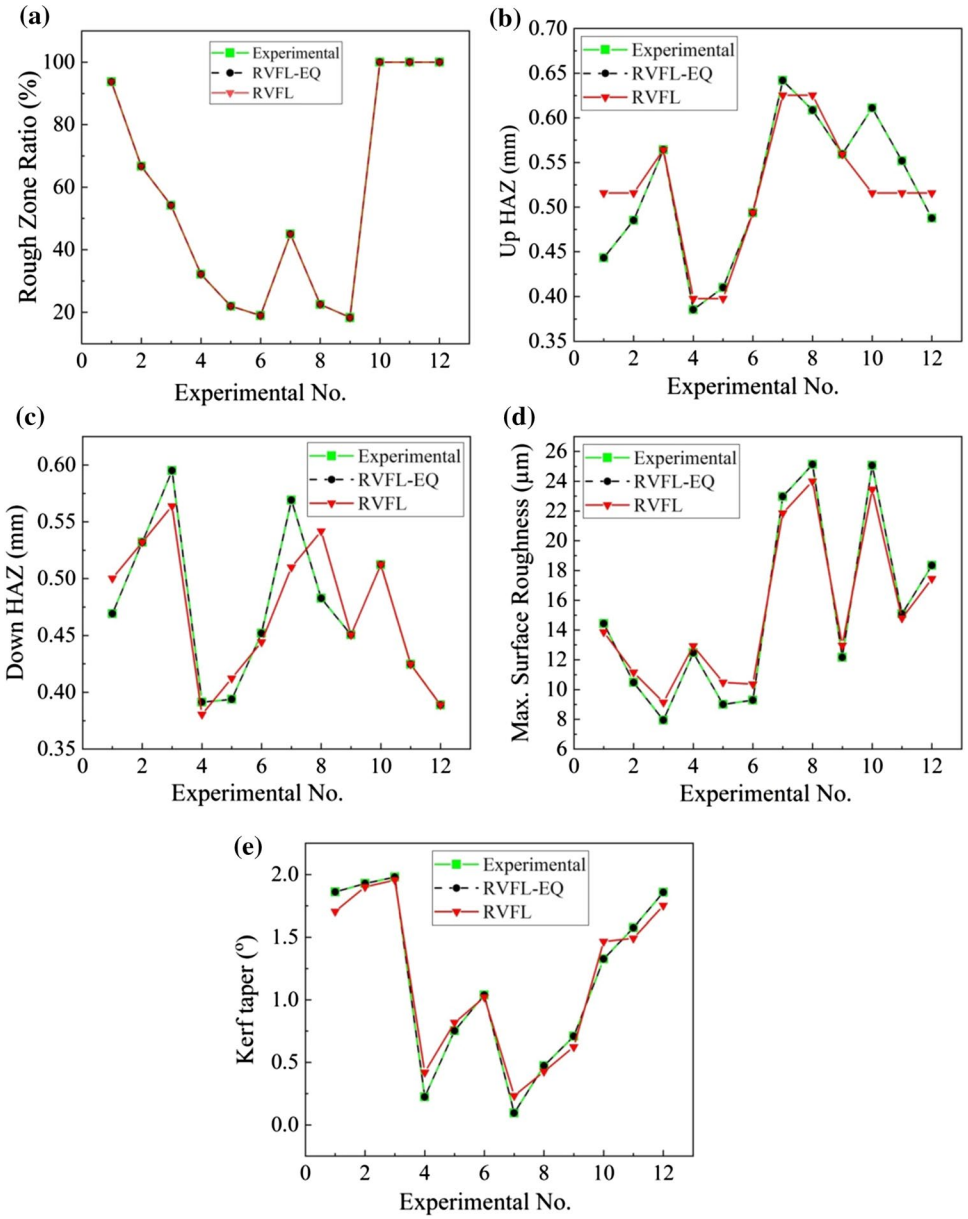

Fig. 7 RVFL and RVFL-EO predicted values versus experimental values for **a** rough zone ratio, **b** UP HAZ, **c** down HAZ, **d** max surface roughness, and **e** Kerf taper angle

in Table 3 was constructed and experiments were performed according to it.

Kerf quality indices

Five kerf quality indices (rough zone ratio, up HAZ, down HAZ, maximum surface roughness, and kerf taper angle) have been considered as responses in the current investigation. The kerf geometry (top kerf width and bottom kerf width) as well as HAZ width has been measured using a polarized light microscope (BH200P) with a color corrected infinity optical system. The surface roughness of the kerf surface was measured using 3D laser scanning confocal microscope (KEYENCE VK-X100). As shown in Fig. 4, the top kerf is wider than the bottom kerf and hence a kerf with a positive taperness is obtained for all conducted experiments. That is due to that the top surface of the sheet is subjected to a large amount of heat compared with the bottom surface, which results in increasing the amount of melting material and consequently the kerf width. The roughness of the top portion of the kerf is larger than that of the bottom portion of the kerf. That is due to that the top portion of the kerf is subjected to the shielding gas for longer period compared to that of the bottom portion, which results in swirling the molten material in the overheated top portion and consequently a surface with bad texture is formed. The shielding gas helps in cooling the top surface of the sheet and consequently the down HAZ is wider than the up HAZ. Rough zone area is another important quality index that was investigated in this study. As shown in Fig. 5, during laser cutting of PMMA

Table 4 Statistical coefficient of performance for RVFL-EO and RVFL

	Rough zone ratio		Up HAZ		Down HAZ		Max. surface roughness (μm)		Kerf taper angle	
	RVFL-EO	RVFL	RVFL-EO	RVFL	RVFL-EO	RVFL	RVFL-EO	RVFL	RVFL-EO	RVFL
R2	0.954	0.943	0.972	0.937	0.991	0.959	0.961	0.958	0.977	0.915
RMSE	15.256	17.071	0.077	0.115	0.057	0.120	3.534	3.655	0.109	0.210
MRE	0.020	0.040	0.029	0.141	0.007	-0.135	0.030	0.042	-0.069	0.021
MAE	10.716	13.456	0.071	0.097	0.051	0.095	3.174	3.316	0.056	0.165
COV	24.625	25.358	16.648	22.679	9.813	23.898	20.401	20.697	16.714	28.747
EC	0.648	0.559	− 1.011	− 3.515	0.558	− 0.923	0.117	0.055	0.095	− 2.347
OI	0.718	0.661	− 0.251	− 1.626	0.662	− 0.205	0.409	0.373	0.382	− 0.992

sheet the roughness of kerf surface varies across the sheet thickness. Three main zones are formed on the kerf surface: rough, transient, and smooth zones. The rough zone is formed near the top surface of the sheet while the smooth zone is formed near the bottom surface of the sheet. The rough zone ratio is defined as the ratio between the rough zone length and the smooth zone length. Figure 6 shows the surface texture of the rough zone of four experiments; two of them have the lowest surface roughness (experiments 3 and 5) and the others have the highest surface roughness (experiments 10 and 17).

Results and discussion

Adequacy of the RVFL-EO model

The RVFL-EO technique has been successfully applied to predict (rough zone ratio, up HAZ, down HAZ, maximum surface roughness, and kerf taper angle) for CO_2 laser cutting processes of PMMA. A superior prediction accuracy of the model can be observed. In order to confirm the strength of the proposed model, RVFL technique was used to predict the same output responses and both results were compared with experimental data. An excellent prediction capability for the RVFL-EO model was observed compared with that of RVFL model as shown in Fig. 7a–e.

Model validation

In order to validate the model, six samples were randomly tested using the proposed EO-RVFL model and RVFL model. The attained results by different models are checked by means of different statistical criteria such as the coefficient of determination (R^2), the root mean square error (RMSE), the mean relative estimate error (MRE), the mean absolute error (MAE), the coefficient of variance (COV), efficiency coefficient (EC), and overall index (OI) (Elsheikh et al. 2019) as shown in Table 4. For the RVFL-EO model, R^2 is 0.954, 0.972, 0.991, 0.961, and 0.977 for rough zone ratio, up HAZ, down HAZ, maximum surface roughness, and kerf taper angle, respectively, while R2 for RVFL model is 0.943, 0.937, 0.959, 0.958, and 0.915 for the same outputs responses, which indicates a great correlation between the experimental and the predicted data of RVFL-EO model compared with the RVFL model. Moreover, the RMSE of RVFL-EO model for all output responses is lower than the RVFL model. Additionally, MRE, MAE, COV, EC, and OI values of RVFL-EO model are lower than that of the RVFL model, and therefore the EO-RVFL technique prediction has great sufficiency to predict the responses of CO_2 laser cutting processes of PMMA with high accuracy.

Conclusion

CO_2 laser cutting process of PMMA sheet has been investigated in this study. Four input factors were included: the gas pressure, the sheet thickness, the laser power, and the cutting speed. Five kerf quality indices were considered as process responses: rough zone ratio, widths of up and down heat affected zones, maximum surface roughness, and kerf taper angle. Taguchi L18 orthogonal array was constructed and experiments were performed according to it. The laser cutting of PMMA forms a tapered kerf that has a wider open on the up surface compared with down surface. The kerf surface has three main regions: rough, transient, and smooth. The rough region is adjacent to the top surface, while the smooth region is adjacent to bottom surface. An enhanced RVFL algorithm integrated with EO algorithm was trained using experimental data to predict the kerf quality indices. The EO algorithm was utilized to obtain the optimal internal parameters of RVFL that maximize its prediction capability. The results obtained by modified RVFL-EO algorithm were compared with those obtained by conventional RVFL as well as experimental ones. Seven statistical criteria (R^2, RMSE, MRE, MAE, COV, EC, and OI) were applied to evaluate the algorithms accuracy. For all investigated kerf quality

indices, RVFL-EO showed a better performance compared with RVFL. These statistical criteria results show the outperformance of RVFL-EO in predicting different kerf quality indices. The following conclusions can be drawn:

- For all conducted experiments, the top kerf width is wider than the bottom kerf width due to the top surface of the sheet is subjected to a large amount of heat compared with the bottom surface, which results in increasing the amount of melting material and consequently the kerf width.
- The roughness of the top portion of the kerf is larger than that of the bottom portion due to the top portion of the kerf is subjected to the shielding gas for longer period which results in swirling the molten material in the overheated top portion and consequently a surface with bad texture is formed.
- The down HAZ is wider than the up HAZ due to the convection cooling via the shielding gas on the top surface.
- The developed RVFL-EO model can be used to predict all kerf quality indices with excellent coefficient of determination ranged between 0.954 and 0.991.
- EO succeeded to obtain the optimal RVFL parameters and consequently enhances the model performance.

Therefore, it is recommended to use RVFL-EO as a predicting tool of the investigated cutting process without involving in conducting more costly time-consuming experiments.

References

Alizadeh, A., & Omrani, H. (2019). An integrated multi response Taguchi- neural network- robust data envelopment analysis model for CO2 laser cutting. *Measurement, 131,* 69–78. https://doi.org/10.1016/j.measurement.2018.08.054.

Babikir, H. A., Elaziz, M. A., Elsheikh, A. H., Showaib, E. A., Elhadary, M., Wu, D., et al. (2019). Noise prediction of axial piston pump based on different valve materials using a modified artificial neural network model. *Alexandria Engineering Journal, 58*(3), 1077–1087. https://doi.org/10.1016/j.aej.2019.09.010.

Bai, H. Z. (2004). Technology SMMJJoMP Experimental and theoretical analyses of cutting nonmetallic materials by low power CO_2-laser. *Journal of Materials Processing Technology, 146*(2), 188–192.

Bao, T., Wang, J., & Yao, Y. J. S. C. T. S. (2010). A fiber optic sensor for detecting and monitoring cracks in concrete structures. *Science China Technological Sciences, 53*(11), 3045–3050. https://doi.org/10.1007/s11431-010-4111-4.

Caiazzo, F., Curcio, F., & Daurelio, G. (2005). Technology FMCMJJoMP Laser cutting of different polymeric plastics (PE, PP and PC) by a CO_2 laser beam. *Journal of Materials Processing Technology, 159*(3), 279–285.

Chaki, S., Bathe, R. N., Ghosal, S., & Padmanabham, G. (2018). Multi-objective optimisation of pulsed Nd:YAG laser cutting process using integrated ANN–NSGAII model. *Journal of Intelligent Manufacturing, 29*(1), 175–190. https://doi.org/10.1007/s10845-015-1100-2.

Chien, W.-T., & Hou, S.-C. (2007). Investigating the recast layer formed during the laser trepan drilling of Inconel 718 using the Taguchi method. *The International Journal of Advanced Manufacturing Technology, 33*(3–4), 308–316.

Choudhury, I. A., & Shirley, S. (2010). Laser cutting of polymeric materials: An experimental investigation. *Optics & Laser Technology, 42*(3), 503–508.

D'Addona, D. M., Genna, S., Leone, C., & Matarazzo, D. (2016). Prediction of poly-methyl-methacrylate laser milling process characteristics based on neural networks and fuzzy data. *Procedia CIRP, 41,* 981–986. https://doi.org/10.1016/j.procir.2016.01.029.

Davim, J. P. (2013). Nontraditional machining processes. In *Manufacturing process selection handbook*, pp. 205–226

Davim, J. P., Barricas, N., Conceicao, M., & Oliveira, C. (2008a). Some experimental studies on CO_2 laser cutting quality of polymeric materials. *Journal of Materials Processing Technology, 198*(1–3), 99–104.

Davim, J. P., Oliveira, C., Barricas, N., & Conceição, M. (2008b). Evaluation of cutting quality of PMMA using CO2 lasers. *The International Journal of Advanced Manufacturing Technology, 35*(9), 875–879. https://doi.org/10.1007/s00170-006-0766-1.

Dubey, A. K., & Yadava, V. (2008a). Laser beam machining: A review. *International Journal of Machine Tools and Manufacture, 48*(6), 609–628.

Dubey, A. K., & Yadava, V. (2008b). Multi-objective optimization of Nd: YAG laser cutting of nickel-based superalloy sheet using orthogonal array with principal component analysis. *Optics and Lasers in Engineering, 46*(2), 124–132.

Elaziz, M. A., Elsheikh, A. H., & Sharshir, S. W. (2019). Improved prediction of oscillatory heat transfer coefficient for a thermoacoustic heat exchanger using modified adaptive neuro-fuzzy inference system. *International Journal of Refrigeration, 102,* 47–54. https://doi.org/10.1016/j.ijrefrig.2019.03.009.

Elsheikh, A. H., Deng, W., & Showaib, E. A. (2019a). Improving laser cutting quality of polymethylmethacrylate sheet: Experimental investigation and optimization. *Journal of Materials Research and Technology*. https://doi.org/10.1016/j.jmrt.2019.11.059.

Elsheikh, A. H., Guo, J., Huang, Y., Ji, J., & Lee, K.-M. (2018). Temperature field sensing of a thin-wall component during machining: Numerical and experimental investigations. *International Journal of Heat and Mass Transfer, 126,* 935–945. https://doi.org/10.1016/j.ijheatmasstransfer.2018.06.006.

Elsheikh, A. H., Sharshir, S. W., Abd Elaziz, M., Kabeel, A. E., Guilan, W., & Haiou, Z. (2019b). Modeling of solar energy systems using artificial neural network: A comprehensive review. *Solar Energy, 180,* 622–639. https://doi.org/10.1016/j.solener.2019.01.037.

Elsheikh, A. H., Sharshir, S. W., Ismail, A. S., Sathyamurthy, R., Abdelhamid, T., Edreis, E. M. A., et al. (2020). An artificial neural network based approach for prediction the thermal conductivity of nanofluids. *SN Applied Sciences, 2*(2), 235. https://doi.org/10.1007/s42452-019-1610-1.

Elsheikh, A., Showaib, E., & Asar, A. (2013). Artificial neural network based forward kinematics solution for planar parallel manipulators passing through singular configuration. *Advances in Robotics & Automation, 2*(106), 2.

Ergur, H. S., & Oysal, Y. (2015). Estimation of cutting speed in abrasive water jet using an adaptive wavelet neural network. *Journal of Intelligent Manufacturing, 26*(2), 403–413. https://doi.org/10.1007/s10845-013-0798-y.

Essa, F. A., Abd Elaziz, M., & Elsheikh, A. H. (2020). An enhanced productivity prediction model of active solar still using artificial neural network and Harris Hawks optimizer. *Applied Thermal Engineering, 170,* 115020. https://doi.org/10.1016/j.applthermaleng.2020.115020.

Faramarzi, A., Heidarinejad, M., Stephens, B., & Mirjalili, S. (2019). Equilibrium optimizer: A novel optimization algorithm. *Knowledge-Based Systems*. https://doi.org/10.1016/j.knosys.2019.105190.

Gautam, G. D., & Pandey, A. K. (2018). Teaching learning algorithm based optimization of kerf deviations in pulsed Nd: YAG laser cutting of Kevlar-29 composite laminates. *Infrared Physics & Technology, 89,* 203–217.

Gonzalez-Val, C., Pallas, A., Panadeiro, V., & Rodriguez, A. (2020). A convolutional approach to quality monitoring for laser manufacturing. *Journal of Intelligent Manufacturing, 31*(3), 789–795. https://doi.org/10.1007/s10845-019-01495-8.

Huang, M., Chen, K.-S., & Hung, Y. (2002). Integrated process capability analysis with an application in backlight module. *Microelectronics Reliability, 42*(12), 2009–2014.

Huang, Z., Zhu, J., Lei, J., Li, X., & Tian, F. (2020). Tool wear predicting based on multi-domain feature fusion by deep convolutional neural network in milling operations. *Journal of Intelligent Manufacturing, 31*(4), 953–966. https://doi.org/10.1007/s10845-019-01488-7.

Jagadish, Bhowmik S., & Ray, A. (2019). Prediction of surface roughness quality of green abrasive water jet machining: A soft computing approach. *Journal of Intelligent Manufacturing, 30*(8), 2965–2979. https://doi.org/10.1007/s10845-015-1169-7.

Kim, G. (2005). A PMMA composite as an optical diffuser in a liquid crystal display backlighting unit (BLU). *European Polymer Journal, 41*(8), 1729–1737.

Kurt, M., Kaynak, Y., Bagci, E., Demirer, H., & Kurt, M. (2009). Dimensional analyses and surface quality of the laser cutting process for engineering plastics. *The International Journal of Advanced Manufacturing Technology, 41*(3–4), 259–267.

Leal-Junior, A. G., Frizera, A., Theodosiou, A., Díaz, C., Jimenez, M., Min, R., et al. (2019). Plane-by-plane written, low-loss polymer optical fiber bragg grating arrays for multiparameter sensing in a smart walker. *IEEE Sensors Journal, 19*(20), 9221–9228.

Leal-Junior, A., Theodosiou, A., Díaz, C., Marques, C., Pontes, M., Kalli, K., et al. (2018a). Fiber Bragg Gratings in CYTOP fibers embedded in a 3D-printed flexible support for assessment of human–robot interaction forces. *Materials, 11*(11), 2305.

Leal-Junior, A. G., Theodosiou, A., Marques, C., Pontes, M. J., Kalli, K., & Frizera, A. (2018b). Compensation method for temperature cross-sensitivity in transverse force applications with FBG sensors in POFs. *Journal of Lightwave Technology, 36*(17), 3660–3665.

Lum, K., Ng, S., & Black, I. (2000). CO_2 laser cutting of MDF: 1. Determination of process parameter settings. *Optics & Laser Technology, 32*(1), 67–76.

Mathew, J., Goswami, G., Ramakrishnan, N., & Naik, N. (1999). Parametric studies on pulsed Nd: YAG laser cutting of carbon fibre reinforced plastic composites. *Journal of Materials Processing Technology, 89,* 198–203.

Prakash, S., & Kumar, S. (2017). Experimental investigations and analytical modeling of multi-pass CO_2 laser processing on PMMA. *Precision Engineering, 49,* 220–234. https://doi.org/10.1016/j.precisioneng.2017.02.010.

Prakash, S., & Kumar, S. (2018). Pulse smearing and profile generation in CO_2 laser micromachining on PMMA via raster scanning. *Journal of Manufacturing Processes, 31,* 116–123. https://doi.org/10.1016/j.jmapro.2017.11.003.

Rao, R., & Yadava, V. (2009). Multi-objective optimization of Nd: YAG laser cutting of thin superalloy sheet using grey relational analysis with entropy measurement. *Optics & Laser Technology, 41*(8), 922–930.

Salman, Kh, Elsheikh, A. H., Ashham, M., Ali, M. K. A., Rashad, M., & Haiou, Z. (2019). Effect of cutting parameters on surface residual stresses in dry turning of AISI 1035 alloy. *Journal of the Brazilian Society of Mechanical Sciences and Engineering, 41*(8), 349. https://doi.org/10.1007/s40430-019-1846-0.

Sharma, A., & Yadava, V. (2011). Optimization of cut quality characteristics during Nd: YAG laser straight cutting of Ni-based superalloy thin sheet using grey relational analysis with entropy measurement. *Materials and Manufacturing Processes, 26*(12), 1522–1529.

Sharma, A., Yadava, V., & Rao, R. (2010). Optimization of kerf quality characteristics during Nd: YAG laser cutting of nickel based superalloy sheet for straight and curved cut profiles. *Optics and Lasers in Engineering, 48*(9), 915–925.

Shehabeldeen, T. A., Elaziz, M. A., Elsheikh, A. H., Hassan, O. F., Yin, Y., Ji, X., et al. (2020). A novel method for predicting tensile strength of friction stir welded AA6061 aluminium alloy joints based on hybrid random vector functional link and henry gas solubility optimization. *IEEE Access, 8,* 79896–79907. https://doi.org/10.1109/ACCESS.2020.2990137.

Shehabeldeen, T. A., Elaziz, M. A., Elsheikh, A. H., & Zhou, J. (2019). Modeling of friction stir welding process using adaptive neuro-fuzzy inference system integrated with harris hawks optimizer. *Journal of Materials Research and Technology, 8*(6), 5882–5892. https://doi.org/10.1016/j.jmrt.2019.09.060.

Showaib, E. A., & Elsheikh, A. H. (2020). Effect of surface preparation on the strength of vibration welded butt joint made from PBT composite. *Polymer Testing, 83,* 106319. https://doi.org/10.1016/j.polymertesting.2019.106319.

Shrivastava, P. K., & Pandey, A. K. (2018). Parametric optimization of multiple quality characteristics in laser cutting of Inconel-718 by using hybrid approach of multiple regression analysis and genetic algorithm. *Infrared Physics & Technology, 91,* 220–232. https://doi.org/10.1016/j.infrared.2018.04.013.

Volpe, A., Trotta, G., Krishnan, U., & Ancona, A. (2019). Prediction model of the depth of the femtosecond laser micro-milling of PMMA. *Optics & Laser Technology, 120,* 105713. https://doi.org/10.1016/j.optlastec.2019.105713.

Wang, X., Li, Z., Chen, T., Lok, B., & Low, D. (2008). 355 nm DPSS UV laser cutting of FR4 and BT/epoxy-based PCB substrates. *Optics and Lasers in Engineering, 46*(5), 404–409.

Zhang, P.-B., & Yang, Z.-X. (2020). A new learning paradigm for random vector functional-link network: RVFL+. *Neural Networks, 122,* 94–105. https://doi.org/10.1016/j.neunet.2019.09.039.